J Mater Sci (2011) 46:2456–2466
DOI 10.1007/s10853-010-5092-1

The influence of $BaGeO_3$ on the properties of $Ba(Ti_{1-x}Sn_x)O_3$ ceramics on the basis of sol-gel powders

Mandy Zenkner · Roberto Köferstein · Stefan G. Ebbinghaus · Lothar Jäger

Received: 20 July 2010 / Accepted: 16 November 2010 / Published online: 3 December 2010

Abstract $Ba(Ti_{1-x-y}Sn_xGe_y)O_3$ (BTSG-*x*-*y*; $x = 0$, 0.05; $y = 0$–0.05) powders were synthesized by a sol-gel (SG) method and for comparative purposes also by a mixed-oxide (MO) method. In this system, $BaGeO_3$ functions as sintering additive. Due to smaller particle sizes of the SG powders a higher sintering activity was found, which resulted in reduced grain growth and in a more homogenous grain size distribution for the corresponding ceramics. The dependence on the paraelectric ⇆ ferroelectric phase transition, i.e. the phase transition temperature, the width of the transition region and completeness were examined by dielectric measurements, DTA as well as by SEM, EDX and XRD investigations with respect to the $BaGeO_3$ content, synthesis method and sintering temperature. The phase transition temperatures of the SG ceramics are remarkably higher than those of the MO ceramics with the same nominal compositions. The reason is a lower tin concentration within the grains of SG ceramics as confirmed by EDX and XRD investigations. The presence of $BaGeO_3$ in barium titanate–stannate system on the basis of a SG method caused an improved incorporation of tin in the $BaTiO_3$ lattice.

M. Zenkner · S. G. Ebbinghaus · L. Jäger (✉)
Institute of Chemistry, Martin-Luther-University Halle-Wittenberg, Kurt-Mothes-Str. 2, 06120 Halle, Germany
e-mail: lothar.jaeger@chemie.uni-halle.de

R. Köferstein
Department of Environmental Engineering, Helmholtz Centre for Environmental Research, UFZ, Permoserstr. 15, 04318 Leipzig, Germany

Introduction

Solid solutions of $BaTi_{1-x}Sn_xO_3$ (BTS-*x*) are well-known as materials for technical applications due to their ferroelectric [1–7] and electromechanical properties [8–10]. BTS-*x* can be used in capacitors, transducers, sensors or actuators. Replacing Ti^{4+} by Sn^{4+} leads to a diffuse paraelectric ⇆ ferroelectric phase transition, which is shifted linearly to lower temperatures with a rate of roughly 8 °C/mol% tin compared to pure $BaTiO_3$ [7]. Furthermore, for the $Ba(Ti_{1-x}Sn_x)O_3$ ceramics, the values of the permittivity maxima increase up to 12.5 mol% tin and decrease for higher tin concentrations [1–3, 10]. The ferroelectric properties have been well investigated for ceramics prepared on the basis of mixed-oxide (MO) powders [1–7, 11–13]. In contrast, ceramics from powders prepared by wet chemical methods have barely been studied although they are expected to have improved properties: nanoscaled powders are obtained with homogenous particle morphologies at low temperatures, higher sintering activity and well-controllable stoichiometry on the atomic scale [14–16].

A survey of the literature on BTS-*x* shows that the dielectric properties of the ceramics strongly vary with the applied synthesis method. Recently, we reported on BTS-*x* powders prepared from the 1,2-ethandiolato complexes $[Ba(C_2H_6O_2)_4][Ti_{1-x}Sn_x(C_2H_4O_2)_3]$ ($x = 0$–1) [17]. In addition, the ferroelectric and electromechanical properties of BTS-0.05 ceramics, obtained from this 1,2-ethandiolato precursor, were investigated by Geske et al. [18]. Furthermore, Kutty et al. [19, 20] described a hydrothermal method (conducted at 280 °C) for solid solutions of the type $Ba(Ti_{1-x}Sn_x)O_3$ up to a Sn content of 35 mol%. Above this tin concentration, a mixture of cubic $BaTiO_3$ and $BaSn(OH)_6{\cdot}3H_2O$ was observed as pre-ceramic powder, which forms mixed crystals after thermal treatment.

Moreover, Du et al. [21] investigated the dielectric properties of $Ba(Ti_{1-x}Sn_x)O_3$ ceramics based on a sol-gel (SG) process starting from dibutyltin dilaurate $[(C_4H_9)_2Sn(C_{12}H_{22}O_2)_2]$ and titanium alkoxide as precursor. Cernea et al. [22, 23] characterized BTS-0.13 ceramics in dependence on the pressing and sintering method, whereas the pre-ceramic powder was obtained by coprecipitation of the corresponding oxalates.

As sintering additive $BaGeO_3$ has already been explored for $BaTiO_3$ or $BaSnO_3$ ceramics [24–28]. By adding of $BaGeO_3$ the sintering process can be carried out at relatively low temperatures, yielding to an extensive suppression of the grain growth. Only few reports deal with the characterization of the $BaTiO_3$–$BaGeO_3$ system. Guha and Kolar [29] described the phase diagram of this system and found that solid solutions were only formed up to 1.8 mol% $BaGeO_3$ in $BaTiO_3$ because of the different ionic radii of Ti^{4+} and Ge^{4+} which results in deviating crystal structures of $BaTiO_3$ (perovskite) and $BaGeO_3$ (pseudowollastonite or pyroxene). Guha and Kolar did not observe any influence of $BaGeO_3$ on the cubic ⇆ tetragonal phase transition temperature determined by X-ray diffraction (XRD) investigations. Furthermore, Plessner et al. [24] found a reduction of the permittivity maximum and a smearing of the paraelectric ⇆ ferroelectric phase transition after substitution of 10 mol% $BaTiO_3$ by $BaGeO_3$. Recently, we reported on the influence of 10 mol% $BaGeO_3$ on the sintering behaviour, shrinkage mechanism, phase evolution and dielectric properties of fine $BaTiO_3$ powders fabricated on the basis of 1,2-ethandiolato precursor [26, 30, 31].

In a previous work [32], we characterized nanocrystalline $Ba(Ti_{1-x-y}Sn_xGe_y)O_3$ (BTSG-*x*-*y*; $x = 0$–0.10; $y = 0$–0.05) powders prepared by a SG method. A higher sintering activity of the SG powders due to the smaller particle sizes compared to the corresponding MO powder led to a stronger densification at lower sintering temperatures. The substitution of $BaTiO_3$ by at least 2 mol% $BaGeO_3$ in the BTSG-0.05-*y* resulted in dense ceramics even at 1,050 °C [i.e. below the formation of a liquid phase ($T \geq 1{,}180$ °C)] with slightly grown grains and a narrow grain size distribution between 0.3 and 1.5 μm.

In this article, we report on the influence of chemical composition and sintering temperature on the dielectric properties and phase transition of BTSG-*x*-*y* ($x = 0$–0.05, $y = 0$–0.05) ceramics. The starting powders were synthesized by a SG method and for comparison also by the MO method.

Experimental

Preparation of BTSG-*x*-*y* by the sol-gel method

The preparation of fine BTSG-*x*-*y* powders has been described in detail in Ref. [32]. Briefly, a mixture of titanium tetrachloride, tin tetrachloride and germanium tetrachloride was dissolved in ethanol at 0 °C. To this mixture, a solution of barium chloride dihydrate was slowly added. This step was followed by a rapid addition of potassium hydroxide dissolved in water. Finally, the mixture was refluxed for 6 h, filtered off using a 200 nm cellulose membrane filter. The product was washed three times with 50 mL deionized water, twice with 50 mL methanol and twice with acetone and afterwards dried at room temperature. The yield was 14.20–14.90 g which decreased to 13.50–14.00 g after calcination at 1,000 °C (96.5–98.1% of theory, related to the initial weight of the element chlorides). The as-prepared powders obtained after drying at room temperature were used for the ceramic preparation.

Preparation of BTSG-*x*-*y* by the mixed-oxide method

The preparation procedure, which has been described in [32], was modified to improve reproducibility. $BaCO_3$, TiO_2 and SnO_2 were separately milled in distilled water for 24 h to dissolve possible impurities, filtered off and dried at 500 °C. Afterwards, stoichiometric amounts of $BaCO_3$, TiO_2, SnO_2 and GeO_2 were ground together in propan-2-ol with agate balls in a PVC container for 24 h. The mass ratio m_{powder}:m_{balls}:$V_{\text{propan-2-ol}}$ was 1:1:4. The resulting powder was filtered off, dried at 120 °C for 24 h and calcined at 1,100 °C for 2 h.

Fabrication of green bodies

The pre-ceramic powders were milled with zirconia balls in propan-2-ol for 2 h (mass ratio m_{powder}:m_{balls}:$m_{\text{propan-2-ol}} = 1{:}1{:}5$), filtered off and dried at 120 °C for 4 h. Afterwards, the resulting samples were milled with 5 wt% of a saturated solution of polyvinyl alcohol as pressing aid for 24 h. The powders were pressed into discs (6 mm diameter and 1.5–1.7 mm thickness) using a downforce of 2 kN (SG powder) or 3 kN (MO powder) and sintered at various temperatures (1,050–1,400 °C) in air with heating and cooling rates of 10 °C/min and a dwelling time of 1 h.

Analytical methods

An impedance analyzer (*Hewlett Packard*, HP4192A LF) was employed to study the dielectric properties. The real part of the permittivity $\varepsilon_{\text{real}}$ was determined by measuring the susceptance B_{imag} of the admittance B

$$B = \mathrm{i}\omega C = \mathrm{i}\omega\varepsilon_0(\varepsilon_{\text{real}} - \mathrm{i}\varepsilon_{\text{imag}}) \cdot \frac{A}{h} = \omega\varepsilon_0(\varepsilon_{\text{imag}} + \mathrm{i}\varepsilon_{\text{real}}) \cdot \frac{A}{h} = (B_{\text{real}} + \mathrm{i}B_{\text{imag}})$$

$$\varepsilon_{\text{real}} = \frac{h}{\omega A \cdot \varepsilon_0} \cdot B_{\text{imag}}$$

with thickness h, surface area of the pellet A, and $\omega = 2\pi f$ with frequency v. Prior to the measurements the samples were annealed in the paraelectric phase for 2 h at 140 °C. Afterwards, the cooling curves were recorded with a rate of 0.2 °C/min at frequencies of 1 kHz–1 MHz and in the temperature range 140–20 °C with an interval step of 0.15 °C for all measurements. Aluminium was applied as electrode material and contacted with tin foil and copper containing epoxy adhesive.

The cubic ⇆ tetragonal phase transition was analyzed by differential thermal analysis (DTA) using a *Netzsch* STA 449C. The samples were placed in Pt crucibles and a cooling rate of 2 °C/min was applied in flowing air (20 mL/min).

Scanning electron microscope images and energy dispersive X-ray analyses (EDX) were taken on a *Philips* XL30 Environmental Scanning Electron Microscope (ESEM) equipped with an X-ray spectrometer from *Edax*. The grain size distributions were determined using the program *Digital Image Processing System 2.3*.

X-ray powder diffraction data were collected on a D8 diffractometer (*Bruker*) with Cu K_α radiation, a step size of $2\Theta = 0.01°$ and a counting time of 1 s per step (*LynX Eye* detector). The powder patterns were refined with the program *PowderCell 2.4*. An X-ray fluorescence spectrometer SRS 3000 (*Siemens*) was used to determine the chemical composition (cellulose pellets).

Results and discussion

Analytical results

To verify identical composition of the calcined SG and MO powders, quantitative elemental analyses were carried out by X-ray fluorescence. The powders contained the expected amounts of elements with a maximum deviation of 2 wt%. In addition, for the SG powders we found small traces of K_2O (<0.2 wt%), Na_2O (<0.3 wt%) and for the MO powders Na_2O (<0.6 wt%), SrO (<0.1 wt%) as well as Fe_2O_3 (<0.1 wt%).

Dielectric properties and phase transition of BTSG-*x*-*y* ceramics

Figure 1 illustrates the characteristics of the phase transition obtained from the permittivity $\varepsilon_{\text{real}}$ and the DTA signal (please note that in all figures only every 30th data point is represented by one symbol). The diffuseness of the transition was estimated from the full width at half maximum

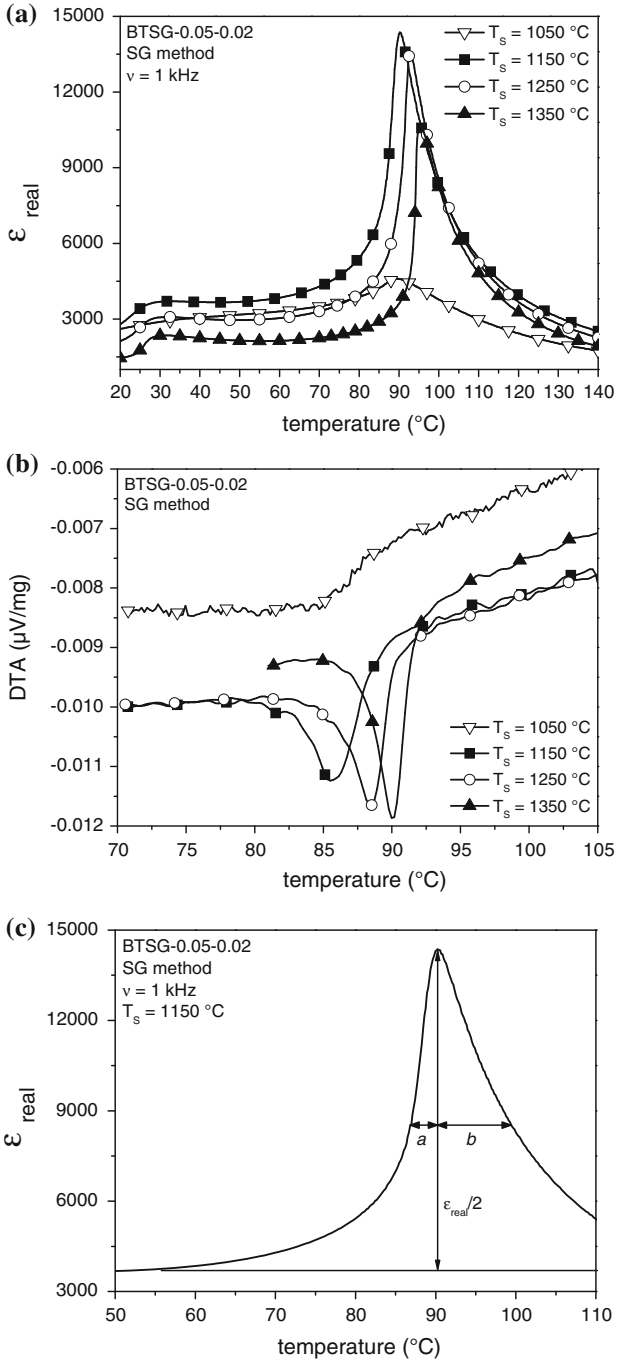

Fig. 1 Phase transitions of BTSG-0.05-0.02 ceramics obtained by the sol-gel method depending on the sintering temperature **a** $\varepsilon_{\text{real}}$, **b** DTA and **c** determination of the diffuseness

of ferroelectric part of the $\varepsilon_{\text{real}}$ curve denoted as '*a*' in Fig. 1c and of the DTA signal. The completeness of the transition can be revealed from the value of $\varepsilon_{\text{real}}$ below the phase transition. The more disordered, non-transformed regions are left the higher $\varepsilon_{\text{real}}$ is. The differences in the phase transition temperatures determined from $\varepsilon_{\text{real}}$ and the DTA signal are due to the different cooling rates applied in

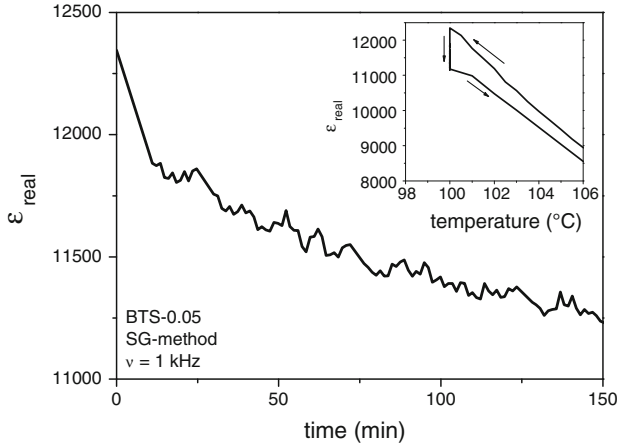

Fig. 2 Time dependence of the dielectric permittivity of a BTS-0.05 ceramic (sol-gel method) at constant temperature of 100 °C. The *inset* shows the temperature dependence

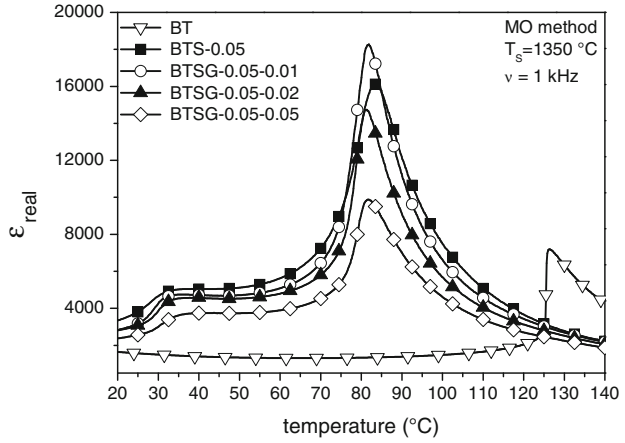

Fig. 3 Real part of permittivity versus temperature for $BaTiO_3$ and BTSG-0.05-*y* ceramics (mixed-oxide method)

the measurements (0.2 and 2 °C/min, see discussion below). Even at the slow cooling rate of 0.2 °C/min the system is not in thermodynamic equilibrium. This becomes evident by interrupting the cooling during the phase transition as shown in Fig. 2. While the isothermal treatment of the sample at 100 °C, ε_{real} decreases by 10% within 150 min indicating a continuation of the transition at this constant temperature. This finding underlines the importance of applying slow heating/cooling rates in the investigation of the phase transition. Unfortunately, this issue is not always taken into account, which may explain deviating values for the transition temperatures reported in the literature. Although our dielectric measurements were carried out with a slow cooling rate of 0.2 °C/min and a narrow step size of 0.15 °C, the absolute ε_{real} values should therefore be treated with some caution.

In Figs. 3 and 4, the influence of the composition of modified $BaTiO_3$ on the dielectric properties of the MO- and SG-based ceramics is shown for unsubstituted $BaTiO_3$ and BTSG-0.05-*y* with $y = 0$, 0.01, 0.02 and 0.05. The ceramics were sintered at 1,350 °C (MO method) and at 1,250 °C (SG method) with an annealing time of 1 h. These sintering temperatures T_S were selected to achieve a relative density of more than 90% for all ceramic bodies (MO and SG). The high densifications at lower sintering temperature of the SG ceramics is caused by a higher sintering activity due to the smaller particle sizes of the SG powders in comparison to the MO powders with identical composition. The substitution of $BaTiO_3$ by at least 2 mol% $BaGeO_3$ in the BTSG-0.05-*y* powders remarkably improves the sintering activity. With this additive, dense ceramics can be obtained even at 1,050 °C [32].

Figure 3 illustrates that the BTS-0.05 ceramic synthesized by the MO method has a much higher permittivity in the whole ferroelectric temperature range than the

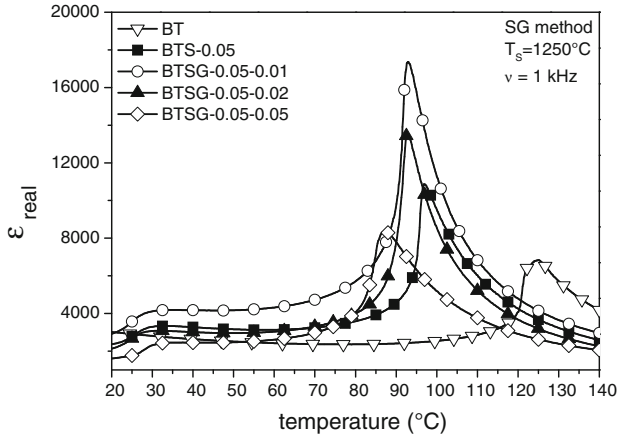

Fig. 4 Real part of permittivity versus temperature for $BaTiO_3$ and BTSG-0.05-*y* ceramics (sol-gel method)

corresponding unsubstituted $BaTiO_3$ ceramic. In addition, the paraelectric ⇆ ferroelectric phase transition temperature (determined from the maximum of the ε_{real} signal) is significantly lowered, resulting in the well-known diffuse phase transition at 83 °C, as reported elsewhere [3, 8, 33]. The substitution of $BaTiO_3$ by $BaGeO_3$ in the BTSG-0.05-*y* ceramics results in a further increase of the permittivity maximum for 1 mol% $BaGeO_3$ ($y = 0.01$) and a reduction of the permittivity maximum for more than 2 mol% $BaGeO_3$ ($y \geq 0.02$) without any significant change of the phase transition temperature (see Table 1). This finding indicates that $BaGeO_3$ does not influence the paraelectric ⇆ ferroelectric phase transition temperature of BTS-0.05, as it was already reported for the Sn-free $BaTiO_3$–$BaGeO_3$ system [24, 29]. The change of the ε_{real} maximum with rising $BaGeO_3$ concentration cannot be explained by grain size effects because all ceramics containing $BaGeO_3$ were found to have an almost identical grain size distribution in

Table 1 Maximum permittivity (ε_{max}), temperature of ε_{max}, phase transition temperature (PTT) determined by DTA, grain size distribution and average grain size, tin content determined by EDX and relative density for BTSG-*x*-*y* ceramics depending on the synthesis method

		ε_{max}	T ε_{max} (°C)	PTT (DTA) (°C)[a]	Grain size (μm)	Ø Grain size (μm)	EDX Sn^{4+} (mol%)	Relative density (%)
$BaTiO_3$	MO	7,200	126.4	124.0	5–20	16	–	92
BTS-0.05	MO	16,200	83.4	82.9	20–120	–	5.1	95
BTSG-0.05-0.01	MO	18,300	81.9	80.7	5–40	18	5.5	96
BTSG-0.05-0.02	MO	14,700	81.1	81.0	4–35	16	5.2	95
BTSG-0.05-0.05	MO	9,900	81.9	79.8	4–40	17	5.5	93
$BaTiO_3$	SG	6,800	125.1	119.4	1–3	2.0	–	95
BTS-0.05	SG	10,900	96.9	95.2	1–6	3.2	3.6	88
BTSG-0.05-0.01	SG	17,400	92.9	90.8	1–8	5.2	3.8	96
BTSG-0.05-0.02	SG	13,500	92.8	90.3	3–23	12	3.9	93
BTSG-0.05-0.05	SG	8,400	87.4	85.7	4–17	13	4.4	93

Ceramics on the basis of mixed-oxide method (MO) sintered at 1,350 °C and sol-gel (SG) method sintered at 1,250 °C for 1 h

[a] Onset temperature

the range from 4 to 40 μm with an average grain sizes of 16–18 μm as can be taken from Table 1. These average grain sizes were determined by the lineal intercept technique for more than 400 grains [34]. A possible reason for the decrease of ε_{real} at higher $BaGeO_3$ contents could be the formation of a liquid phase or the presence of a second crystalline phase. Liquid phase sintering was reported to start at a $BaGeO_3$ concentration above 1.8 mol% [29] at 1,180 °C [32]. Traces of a second phase appear in the XRD pattern for annealed powders (1,200–1,400 °C) possessing a germanium content of 5 mol%. This phase can be attributed to the orthorhombic $BaGeO_3$ (curve a) in Fig. 6 [35]. In this context, it is worth mentioning that for $BaTi_{0.9}Sn_{0.1}O_3$ ceramics doped with B_2O_3, Tawichai et al. [36] reported that the presence of a second phase leads to lower dielectric constants. Furthermore, we found that the ferroelectric part a of the full width at half maximum of the transition region is narrower for the ceramics with 1 mol% ($a = 4.7$ °C) and 2 mol% $BaGeO_3$ ($a = 3.6$ °C) than for the BTS-0.05 ceramic ($a = 6.4$ °C). In addition, for these ceramics (1 and 2 mol% $BaGeO_3$), a stronger decrease of permittivity below the maximum (i.e. at temperatures around 50 °C) indicates a more complete phase transition. The ceramic with 5 mol% $BaGeO_3$ ($a = 4.1$ °C) reveals a more diffuse character than the BTSG-0.05-0.02 ceramic probably caused by the formation of a second crystalline phase.

Figure 4 compares the permittivity of the ceramics obtained by the SG method. The changes of the ε_{real} maxima with the substitution of titanium by tin and with increasing $BaGeO_3$ are similar to those of the corresponding MO ceramics. The values of the ε_{real} maxima for the SG ceramics are only marginally lower than for the corresponding MO ceramics, which may be attributed to different microstructures. The ceramics obtained from the SG powders have a narrower grain size distribution. In particular, the ceramics without the formation of a liquid phase ($y < 0.02$) exhibit a far smaller average grain size (Ø = 2–5 μm, Table 1) than their MO counterparts. In contrast, for the SG ceramics an accelerated grain growth is observed with occurrence of the liquid phase (Ø = 12–13 μm).

The analysis of the phase transition temperatures reveals remarkable differences between the MO and SG ceramics. The transition temperatures are shifted to higher values in comparison to the MO ceramics. For example, the permittivity maximum for the BTS-0.05 ceramic is found at 97 °C, which is 14 °C higher than the one of the corresponding MO ceramic. This higher temperature of the ε_{real} maximum apparently hints at a lower tin concentration in the SG ceramic.

EDX spectroscopy on various grains of the ceramics was carried out in order to determine the local tin content. The tin concentration within the grains of the MO ceramics varied between 5.1 and 5.5 mol%, which corresponds well with the nominal Sn content. However, the grains of BTS-0.05 SG ceramic contain less tin (3.6 mol%) than the expected value of 5 mol% (Table 1) (please note that the corresponding powder contains the nominal value of 5 mol% tin determined by X-ray fluorescence). Under the assumption that a linear decrease of T_C takes place with a rate of roughly 8 °C/mol% tin [7], the EDX result of 3.6 mol% tin is in good agreement with the phase transition temperature of 97 °C.

In addition, a back-scattered electron image coupled with EDX spectroscopy was used to locate the remaining

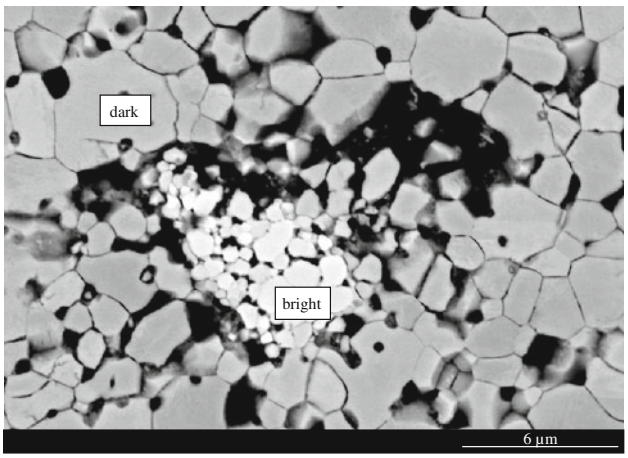

Fig. 5 SEM image (back-scattered electron imaging mode) of a BTS-0.05 ceramic (sol-gel method) sintered at 1,250 °C for 1 h. *Bright grains* have 78 mol% tin content, while *dark grains* exhibit a content of only 3.6 mol%

tin in the ceramic. In Fig. 5, it can be seen that the BTS-0.05 ceramic consists of different grains, appearing bright and dark. These contrasts indicate different compositions. The main phase of dark grains contains about 3.6 mol% Sn. Few local bright areas exist possessing rather small grains. These grains contain approximately 78 mol% tin (EDX). The high content of tin in the second phase is responsible for low grain growth and poor densification observed for these areas [37–39].

Consequently, we tried to attain a more homogenous element distribution by modifying the sintering procedure. Despite of an elongation of the dwelling time up to 80 h at 1,350 °C we did not achieve an uniform graining. The phase transition temperature for the BTS-0.05 ceramic determined by DTA remained unchanged although the sintering time was increased from 1 h (96.5 °C) to 80 h (96.3 °C). Even after repeated crushing and sintering (five times), the ceramics did not show any shift of the DTA signal, indicating that the tin rich phase is thermodynamically stable. Several authors [14–16] claimed that wet chemical methods result in more homogenous and well-stoichiometric powders compared to the MO method. In contrast, we found that the BTS-0.05 ceramics obtained from a MO powder consist of one homogeneous phase, while ceramics based on a SG powder contain two phases with different compositions as determined by EDX. The main phase dominates the dielectric properties of the ceramic. Concerning the phase transition temperature for BTS-0.05, values of about 82 °C were reported for MO ceramics [3, 8, 33, 40]. On the other hand, for a SG ceramic the transition temperature amounts to 95 °C [21]. Both results were confirmed by our findings. Probably, this broad variation, especially the highest values, are caused by the appearance of a second phase and by an incomplete incorporation of tin leading a wrong tin concentration. In this context, it is worth mentioning that Kutty et al. [19, 20] found that BTS-*x* pre-ceramic powders with a tin content above 35 mol% prepared under hydrothermal conditions consisted of $BaTiO_3$ and $BaSn(OH)_6{\cdot}3H_2O$. After thermal treatment at 1,000 °C these pre-ceramic powders form solid solutions.

A more uniform distribution of tin in the SG ceramics can be achieved by the use of $BaGeO_3$ as additive. With raising $BaGeO_3$ concentration, the phase transition is shifted to lower temperatures, e.g. from 97 °C (BTS-0.05) to 93 °C (BTSG-0.05-0.01) to 87 °C (BTSG-0.05-0.05), respectively (Fig. 4). The reason for this shift is the increasing tin concentration in the grains of the main phase as determined by EDX measurements. As shown in Table 1, the Sn concentration increase from 3.6 to 4.4 mol% with rising $BaGeO_3$ content. This shows that a higher $BaGeO_3$ concentration supports a more homogenous distribution of tin ions in the $BaTiO_3$ structure (assuming that $BaGeO_3$ itself does not influence the phase transition temperature as proved above for MO ceramics).

The pure $BaTiO_3$ ceramic prepared by the SG method shows a more diffuse character of the phase transition with $a = 4.4$ °C due to the lower average grain size compared to the corresponding MO ceramic with $a = 0.9$ °C (Figs. 3, 4). On the other hand, for the Sn-substituted compounds the ε_{real} signals of the SG samples are less diffuse than those of the corresponding MO ceramics caused by the lower tin concentrations of the main phase in SG ceramics. A comparison of the SG ceramics shows that the width of the phase transition is relatively small for BTS-0.05 ($a = 1.6$ °C), while it increases for the ceramic with 1 mol% $BaGeO_3$ ($a = 2.2$ °C), 2 mol% $BaGeO_3$ ($a = 2.4$ °C) and 5 mol% $BaGeO_3$ ($a = 4.0$ °C). The increase of the diffuse character in the SG ceramics by the addition of $BaGeO_3$ hints at an improved incorporation of tin in the $BaTiO_3$ lattice.

In addition, the XRD pattern of SG and MO powders with equal nominal composition reveal differences in their crystal structures at room temperature. The investigated samples were obtained from the pre-ceramic powders by calcination at different temperatures. As an example, the pattern 'b' in Fig. 6 shows the diffraction pattern of the BTSG-0.05-0.02 powder (MO) calcined at 1,300 °C. The peak splitting, seen in the enlarged XRD regions at approximately $2\Theta \approx 45°$ and 51°, can be assigned to the orthorhombic phase of $BaTiO_3$ [41]. The presence of this phase is in accordance with the $BaTiO_3$–$BaSnO_3$ phase diagram [1, 2]. In contrast, a clearly different diffraction pattern was observed for the SG powder with identical composition after calcination at 1,200 °C (curve 'c' in Fig. 6). The splitting of the characteristic reflections at

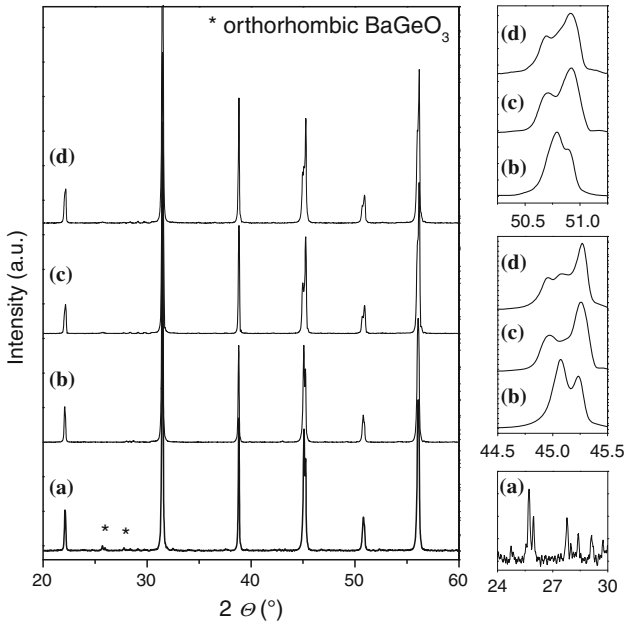

Fig. 6 X-ray diffraction patterns of powders after calcination at different temperatures **a** BTSG-0.05-0.05 (mixed-oxide method) calcined at 1,300 °C, **b** BTSG-0.05-0.02 (mixed-oxide method) calcined at 1,300 °C, **c** BTSG-0.05-0.02 (sol-gel method) calcined at 1,200 °C and **d** BTSG-0.05-0.02 (sol-gel method) calcined at 1,300 °C

$2\Theta \approx 45°$ and 51° can be attributed to the tetragonal crystal structure [41]. An increase of the calcination temperature to 1,300 °C for the SG powder results in three reflections at the Bragg angle 45° according to the coexistence of both the tetragonal and orthorhombic phase (pattern 'd' in Fig. 6). On the basis of a quantitative phase analysis by XRD, the tetragonal to orthorhombic phase ratio for this SG powder is calculated as 56:44 wt%. In BTS-0.05 ceramics, a tetragonal–orthorhombic phase coexistence at room temperature was already reported by Mueller [33]. The phase analysis of our powders obtained by crushing of the sintered ceramics revealed the same phase compositions: a orthorhombic phase for the MO sample sintered at 1,300 °C, a tetragonal phase for the SG sample sintered at 1,200 °C and a tetragonal–orthorhombic phase coexistence for the SG sample sintered at 1,300 °C. In addition, for our samples the cell volume was determined for the SG and MO powders calcined at 1,300 °C. For the MO powder of BTSG-0.05-0.02, a cell volume of $V = 64.569$ Å^3 was calculated, whereas a slightly smaller cell volume of $V = 64.475$ Å^3 was observed for the SG powder. These results confirm the above described lower tin concentration in the main phase of the sample prepared by the SG method. Traces of tin compounds like $BaSnO_3$ or Ba_2SnO_4 were not found in any of the samples.

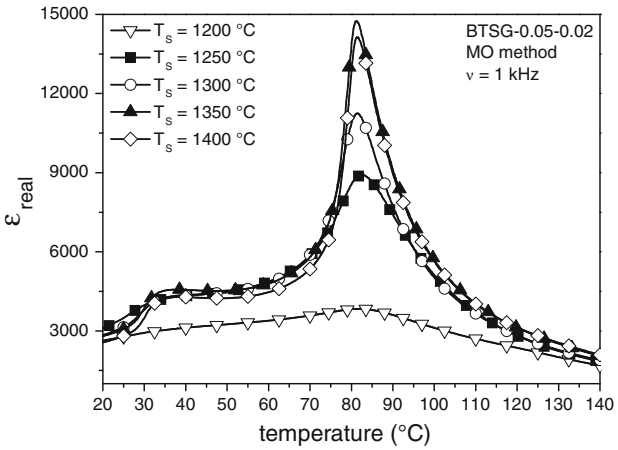

Fig. 7 Real part of permittivity versus temperature for BTSG-0.05-0.02 ceramics (mixed-oxide method) depending on the sintering temperature

Influence of sintering temperature on the phase transition of BTSG-0.05-0.02 ceramics

The dielectric properties of the BTSG-0.05-0.02 (MO and SG) ceramics sintered at different temperatures are shown in Figs. 1 and 7. Rather low values of the permittivity were found for ceramics sintered at 1,200 °C (MO) and 1,050 °C (SG) due to the small grain sizes, which can be seen from the SEM images shown in Fig. 8. The influence of grain size effects has been discussed in Refs. [42–46]. A high porosity as a second possible origin for the observed low ε_{real} values can be excluded because the density of these ceramics was determined to be about 96%.

The general trend observed for the MO ceramics is that the maxima of ε_{real} raise with increasing sintering temperatures because of the resulting larger grain sizes. The permittivity maxima increased from 8,900 for $T_S = 1{,}250$ °C to approximately 14,700 for $T_S = 1{,}350$ °C. The phase transition temperature was found to be approximately 82 °C independent of the sintering temperature (Table 2). With elevated sintering temperature, the full width at half maximum of the transition region and thus the diffuseness of the phase transition decrease from $a = 14.2$ °C ($T_S = 1{,}200$ °C) to $a = 3.5$ °C ($T_S = 1{,}400$ °C).

In contrast to the MO samples, we surprisingly observed a different dependence on the dielectric properties of the sintering temperatures for SG ceramics. Below the formation of the liquid phase ($T > 1{,}180$ °C) the ε_{real} maxima of the SG ceramics increase from 4,600 for $T_S = 1{,}050$ °C to 14,400 for $T_S = 1{,}150$ °C. Comparable values of permittivity maxima were achieved with a lower average grain size for SG ceramics compared to the MO ceramics. For example, an ε_{real} maximum of approximately 14,000 is obtained for the SG ceramic with average grain sizes of 8.7 μm ($T_S = 1{,}150$ °C) and for the MO ceramic with

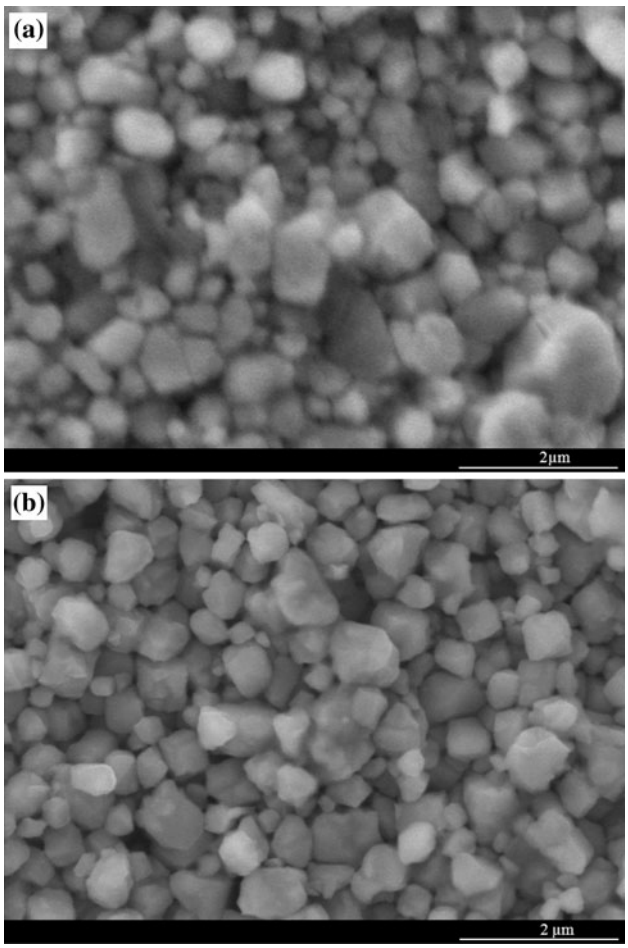

Fig. 8 SEM images of BTSG-0.05-0.02 ceramics sintered at **a** 1,200 °C (mixed-oxide method) and **b** 1,050 °C (sol-gel method) for 1 h

average grain sizes of 20 µm (T_S = 1,400 °C). A further increase of sintering temperature for the SG sample is accompanied by a strong grain growth caused by the formation of a liquid phase that leads to a gradual decline of the ε_{real} maxima.

Moreover, for the SG ceramics, the diffuse character of the transition region considerably decreases with increasing sintering temperature (Fig. 1a). The ferroelectric part of the full width at half maximum is reduced from a = 8.6 °C (T_S = 1,050 °C) to a = 1.7 °C (T_S = 1,350 °C). The same behaviour is observed in the DTA measurements shown in Fig. 1b. The DTA peaks gradually become weaker as well as broader and are shifted to lower temperatures with decreasing grain sizes. This behaviour is associated with a reduction of the transition enthalpy. These results are consistent with earlier reports [46, 47]. The SG ceramics sintered at 1,050 °C (Ø = 0.6 µm) and 1,150 °C (Ø = 8.7 µm) reveal very diffuse and incomplete phase transitions. The permittivity of roughly 3,700 between 30 and 70 °C is very high for the ceramic sintered at 1,150 °C (Fig. 1). A lower value of approximate 3,200 (30–70 °C) as well as the lack of a clear peak in the DTA signal were observed for T_S = 1,050 °C (Ø = 0.6 µm). In agreement with our results, for pure $BaTiO_3$ ceramics a pronounced maximum of the permittivity at room temperature was found for grain sizes between 0.8 and 1 µm [43]. Below this value the permittivity progressively decreases, which is explained by increasing intrinsic and extrinsic effects. The intrinsic contributions include the change of tetragonality (ratio of the cell parameters a and c) with the grain size, whereas the extrinsic effects result from the change of grain boundaries and domain structure [46–48]. In contrast to the samples sintered at 1,050 and 1,150 °C, a low diffuseness and a sharp descent of ε_{real} below the phase transition temperature was obtained for the SG sample sintered at 1,350 °C. The high phase transition enthalpy (Fig. 1b) and the very low ε_{real} value of approximately 2,200 at low temperatures (30–70 °C) indicate a complete phase transition.

Table 2 Maximum permittivity (ε_{max}), temperature of ε_{max}, phase transition temperature (PTT) determined by DTA, grain size distribution, average grain size and relative density for BTSG-0.05-0.02 ceramics depending on the synthesis method and the sintering temperature

T_S (°C)		ε_{max}	T ε_{max} (°C)	PTT (DTA) (°C)[a]	Grain size (µm)	Ø Grain size (µm)	Relative density (%)
1,200	MO	3,800	81.9	–	0.5–2	0.8	96
1,250	MO	8,900	82.5	81.3	2–12	6.6	95
1,300	MO	11,200	81.6	81.1	3–16	8.3	96
1,350	MO	14,700	81.1	81.0	4–35	16	95
1,400	MO	14,100	81.4	79.8	5–45	20	94
1,050	SG	4,600	89.1	–	0.3–1	0.6	97
1,100	SG	13,900	90.1	87.4	2–11	6.0	96
1,150	SG	14,400	90.3	88.8	3–14	8.7	95
1,200	SG	12,900	91.6	89.8	3–20	10	92
1,250	SG	13,500	92.8	90.3	3–23	12	93
1,300	SG	12,200	93.4	90.9	5–50	21	90
1,350	SG	10,700	95.4	91.6	5–85	36	91

Ceramics on the basis of mixed-oxide method (MO) and sol-gel method (SG) were sintered for 1 h

[a] Onset temperature

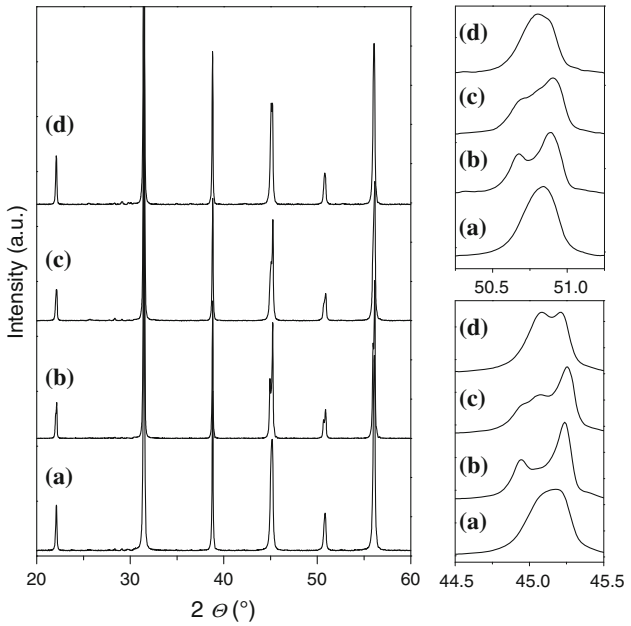

Fig. 9 X-ray diffraction patterns of BTSG-0.05-0.02 ceramics (sol-gel method) sintered at **a** 1,050 °C, **b** 1,150 °C, **c** 1,300 °C and **d** 1,350 °C

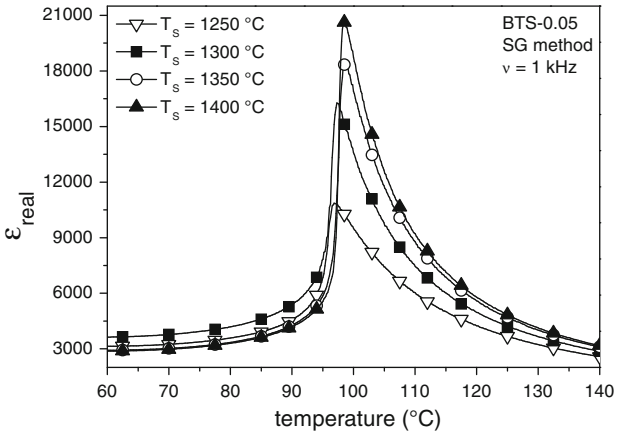

Fig. 10 Real part of permittivity versus temperature for BTS-0.05 ceramics (sol-gel method) depending on the sintering temperature

In addition, XRD analyses of the powders obtained after crushing of the sintered SG ceramics exhibit different phases depending on the sintering temperature. For BTSG-0.05-0.02 samples sintered at 1,050 and 1,150 °C, the XRD pattern changes from (pseudo-)cubic to the tetragonal structure as seen in the diffraction patterns 'a' and 'b' in Fig. 9. For higher sintering temperatures, the ceramics reveal a coexistence of the tetragonal and orthorhombic phase at room temperature indicated by three reflections at the Bragg angle 45° as seen from curve 'c' in Fig. 9. The part of orthorhombic phase increases with rising sintering temperature. The enlarged XRD pattern 'd' clearly shows that the relative intensities of the orthorhombic reflections (on the left side) increase while the intensities of the tetragonal phase decrease (on the right side) in comparison to curve 'c'.

Furthermore, it was noticed that a considerable shift of the paraelectric ⇆ ferroelectric phase transition to higher temperature occurs with increasing sintering temperature for the SG ceramics (Fig. 1). The transition temperature of 89 °C found for T_S = 1,050 °C gradually increases up to 95 °C for T_S = 1,350 °C. This finding cannot be explained by the formation of a liquid phase because we did not observe a similar effect for the corresponding MO ceramics of identical composition. An increase of the phase transition temperatures with increasing sintering temperature was also found for SG samples without $BaGeO_3$ as shown for the sample BTS-0.05 in Fig. 10. In a previous study on unsubstituted $BaTiO_3$ ceramics, Kuwabara et al. [49] also discussed an increase of the Curie temperature with sintering temperature from 125.5 °C (T_S = 1,250 °C) to 129.5 °C (T_S = 1,450 °C). The authors explained this phenomenon by defects in the $BaTiO_3$ lattice caused by acceptor-type impurities. For wet chemically prepared powders, it is known that protons are incorporated as OH^- groups in the perovskite lattice [50, 51]. These defects are compensated by metal vacancies, acceptor impurities or electrons. In our case acceptor impurities as possible reason are unlikely because the same or even higher concentrations of acceptor ions like sodium and iron were detected by elemental analysis in the MO powders. A more likely explanation is a change in density. We found that the decline of the permittivity maxima of BTSG-0.05-0.02 ceramics for sintering temperatures above 1,200 °C is accompanied by a slight decrease of relative densities to values below 95%. Zhao et al. [47] reported that a porosity level >5% leads to a strong depression of the permittivity. Similar trends were also described for BTS-0.10 ceramics doped with 0.5 wt% B_2O_3. For T_S > 1,350 °C, the densities and permittivity maxima of these ceramics decrease [52]. The mentioned porosity effects reported in Refs. [47, 52] may be the reason in our ceramics, too, since the observed decrease of permittivity maxima is accompanied by a reduction of densities to 95–90%.

Furthermore, the cubic ⇆ tetragonal phase transition was studied by DTA for ceramic bodies after sintering. We determined the transition temperatures as the onset point of the cooling curve. The resulting temperatures are lower than the corresponding temperature of ε_{real} maximum due to the faster cooling rates of 2 °C/min. Nevertheless, the DTA results revealed the same tendency with a maximal temperature difference of only 3 °C with exception of the SG sample $BaTiO_3$ (Tables 1, 2).

The phase diagram of BTS-*x* solid solutions was described in Refs. [1, 2]. In contrast to the

cubic ⇆ tetragonal phase transition, the temperatures of the orthorhombic ⇆ tetragonal and the rhombohedral ⇆ orthorhombic phase transitions increase with rising tin content. These transition points coincide at a tin content of around 10 mol%, resulting in the disappearance of the tetragonal and orthorhombic phase. Instead, a direct transition cubic ⇆ rhombohedral is found for tin contents ≥10%. As seen in Figs. 1 and 7, the orthorhombic ⇆ tetragonal transition for the SG and MO ceramics takes place at very different temperatures. The phase transition occurs below 28 °C for the SG ceramics and below 33 °C for the corresponding MO ceramics. This is a further indication that the main phase (grains) of the SG ceramics contains less tin than the nominal value.

Finally, the frequency dependence of ε_{real} was investigated for the MO and SG ceramics sintered at the lowest applicable temperatures (1,200 and 1,050 °C, respectively). Figure 11 shows the permittivity of BTSG-0.05-0.02 ceramics as function of temperature and frequency. A very weak frequency dispersion was observed for both the MO samples (Fig. 11a) and SG samples (Fig. 11b) with the lowest average grain sizes of 0.8 and 0.6 μm, respectively. The difference, $\Delta T = T_{\varepsilon_{max}}(1\,\mathrm{MHz}) - T_{\varepsilon_{max}}(1\,\mathrm{kHz})$, is 0.7 °C for the MO and 0.6 °C for the SG sample.

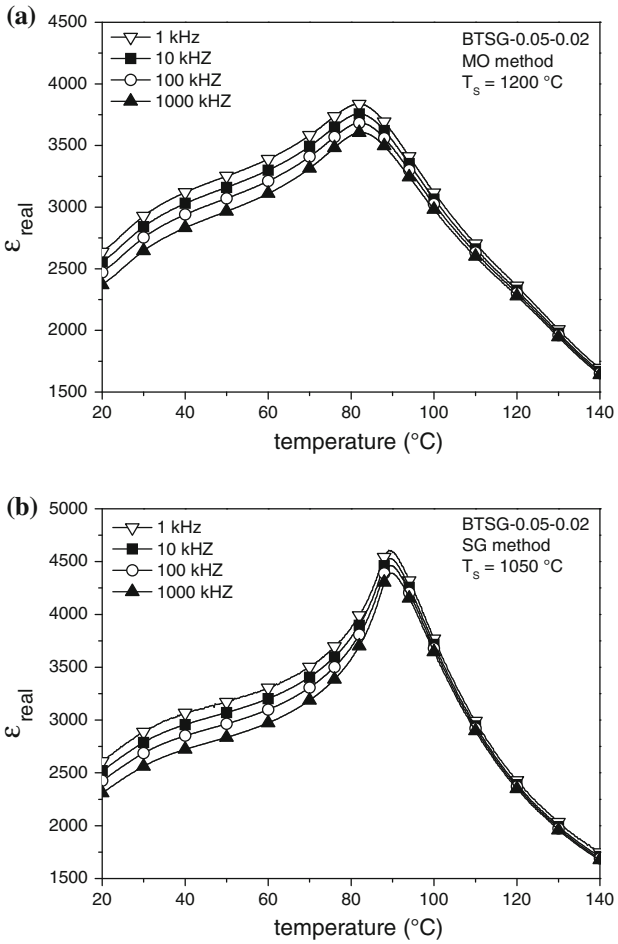

Fig. 11 Real part of permittivity versus temperature for BTSG-0.05-0.02 ceramics depending on frequency **a** mixed-oxide method (T_S = 1,200 °C) and **b** sol-gel method (T_S = 1,050 °C)

Conclusion

In this article, for the first time detailed studies are reported on the influence of the sintering additive $BaGeO_3$ on BTS-0.05 ceramics with respect to the dielectric properties and ferroelectric ⇆ paraelectric phase transition. The preceramic powders were obtained by a SG and the MO method. $BaGeO_3$ is a well-suited additive to obtain highly dense ceramics at clearly lower temperatures. The addition of 2 mol% $BaGeO_3$ resulted in dense ceramics even at 1,050 °C on the basis of a SG and even at 1,150 °C on the basis of the MO powders in comparison to BTS-0.05 ceramics. The paraelectric ⇆ ferroelectric phase transition temperatures for BTSG-*x*-*y* ceramics obtained by a SG method are higher than those of the corresponding MO ceramics because the grains of the SG ceramics consist of different phases with higher and lower tin concentrations, respectively. Only the main phase with the lower tin concentration dominates the dielectric properties and phase transitions. By adding $BaGeO_3$, a more homogenous tin distribution was obtained in the SG ceramics. A higher germanium concentration results in the formation of orthorhombic $BaGeO_3$. Moreover, with increasing sintering temperature the diffuse character of the transition regions gradually decreases and the completeness increase for both SG and MO ceramics. Dense SG ceramics were achieved below the formation of a liquid phase with narrow grain size distribution, which show higher values of permittivity at and below the maximum (T_S = 1,100–1,150 °C).

Acknowledgements We thank Dr. U. Straube und Prof. G. Schmidt (Institute of Physics) for the experimental helps and extended discussions concerning the impedance measurements. This work was supported by the Federal State Saxony-Anhalt (Cluster of Excellence: Nanostructured Materials).

References

1. Smolenskii GA, Isupov VA (1954) Zh Tekh Fiz 24:1375
2. Yasuda N, Ohwa H, Asano S (1996) Jpn J Appl Phys 35:5099
3. Markovic S, Mitric M, Cvjeticanin N, Uskokovic D (2006) Mater Sci Forum 518:241
4. Baskaran N, Chang H (2001) J Mater Sci Mater Electron 12:527
5. Bak W, Kajtoch C, Starzyk F (2003) Mater Sci Eng B 100:9
6. Wang T, Chen XM, Zheng XH (2003) J Electroceram 11:173
7. Wei X, Yao X (2007) Mater Sci Eng B 137:184
8. Oh K-Y, Uchino K, Cross LE (1994) J Am Ceram Soc 77:2809

9. von Cieminski J, Langhammer HT, Abicht H-P (1990) Phys Status Solidi A 120:285
10. Geske L, Beige H, Abicht H-P, Mueller V (2005) Ferroelectrics 314:97
11. Wei X, Feng Y, Yao X (2003) Appl Phys Lett 83:2031
12. Mueller V, Beige H, Abicht H-P (2004) Appl Phys Lett 84:1341
13. Lei C, Bokov AA, Ye Z-G (2007) J Appl Phys 101:084105
14. Abicht H-P, Völtzke D, Müller T (1990) Z Chem 30:385
15. Vijatovic MM, Bobic JD, Stojanovic BD (2008) Sci Sinter 40:155
16. Pithan C, Hennings D, Waser R (2005) Int J Appl Ceram Technol 2:1
17. Köferstein R, Jäger L, Lorenz V, Abicht H-P, Woltersdorf J, Pippel E, Görls H (2005) Solid State Sci 7:1280
18. Geske L, Lorenz V, Müller T, Jäger L, Beige H, Abicht H-P, Mueller V (2005) J Eur Ceram Soc 25:2537
19. Kutty TRN, Vivekanandan R (1987) Mater Res Bull 22:1457
20. Vivekanandan R, Kutty TRN (1988) Ceram Int 14(4):207
21. Du F, Cui B, Cheng H, Niu R, Chang Z (2009) Mater Res Bull 44:1930
22. Cernea M, Manea A, Piazza D, Galassi C, Vasile E (2007) J Am Ceram Soc 90:1728
23. Aldica G, Cernea M, Ganea P (2010) J Mater Sci 45:2606. doi: 10.1007/s10853-010-4234-9
24. Plessner KW, West R (1955) Proc Phys Soc B 68:1150
25. Baxter P, Hellicar NJ, Lewis B (1959) J Am Ceram Soc 42(10):465
26. Köferstein R, Jäger L, Zenkner M, Abicht H-P (2008) J Mater Sci 43:832. doi:10.1007/s10853-007-2195-4
27. Köferstein R, Jäger L, Zenkner M, Müller T, Ebbinghaus SG (2010) J Eur Ceram Soc 30:1419
28. Köferstein R, Jäger L, Zenkner M, Garcia-Garcia FJ, Ebbinghaus SG (2010) J Mater Sci 45:3784. doi:10.1007/s10853-010-4432-5
29. Guha JP, Kolar D (1972) J Mater Sci 7:1192. doi:10.1007/BF00550202
30. Köferstein R, Jäger L, Zenkner M, Müller T, Abicht H-P (2008) Mater Chem Phys 112:531
31. Köferstein R, Jäger L, Zenkner M, Ebbinghaus SG (2010) Mater Chem Phys 119:118
32. Zenkner M, Jäger L, Köferstein R, Abicht H-P (2008) Solid State Sci 10:1556
33. Mueller V, Beige H, Abicht H-P, Eisenschmidt C (2004) J Mater Res 19:2834
34. Wurst JC, Nelson JA (1972) J Am Ceram Soc 55:9
35. PDF2 International Centre of Diffraction Data, Pennsylvania (2001) (37-137 orthorhombic $BaGeO_3$)
36. Tawichai N, Intatha U, Eitssayeam S, Pengpat K, Rujijanagul G, Tunkasiri T (2010) Phase Transit 83:55
37. Wagner G, Binder H (1958) Z Anorg Allg Chem 297:328
38. Upadhyay S, Parkash O, Kumar D (1997) J Mater Sci Lett 16:1330
39. Köferstein R, Jäger L, Zenkner M, Ebbinghaus SG (2009) J Eur Ceram Soc 29:2317
40. Ramesh Babu A, Prasadarao AV (1997) Mater Sci Lett 16:313
41. Kwei GH, Lawson AC, Billinge SJL, Cheong S-W (1993) J Phys Chem 97:2368
42. Kinoshita K, Yamaji A (1976) J Appl Phys 47:371
43. Arlt G, Hennings D, de With G (1985) J Appl Phys 58(4):1619
44. Kanata T, Yoshikawa T, Kubota K (1987) Solid State Commun 62:765
45. Frey MH, Xu Z, Han P, Payne DA (1998) Ferroelectrics 206–207:337
46. Buscaglia V, Buscaglia MT, Viviani M, Mitoseriu L, Nanni P, Trefiletti V, Piaggio P, Gregora I, Ostapchuk T, Pokorny J, Petzelt J (2006) J Eur Ceram Soc 26:2889
47. Zhao Z, Buscaglia V, Viviani M, Buscaglia MT, Mitoseriu L, Testino A, Nygren M, Johnsson M, Nanni P (2004) Phys Rev B 70:024107
48. Buscaglia MT, Viviani M, Buscaglia V, Mitoseriu L, Testino A, Nanni P, Zhao Z, Nygren M, Harnagea C, Piazza D, Galassi C (2006) Phys Rev B 73:064114
49. Kuwabara M, Matsuda H, Kurata N, Matsuyama E (1997) J Am Ceram Soc 80:2590
50. Waser R (1988) J Am Ceram Soc 71:58
51. Hennings D, Schreinemacher S (1992) J Eur Ceram Soc 9:41
52. Tawichai N, Rujijanagul G (2009) Ferroelectrics 385:128